2D Titanium Carbide ($Ti_3C_2T_x$) in Accommodating Intraocular Lens Design

*Emma J. Ward, Joseph Lacey, Cyril Crua, Marcus K. Dymond, Kathleen Maleski, Kanit Hantanasirisakul, Yury Gogotsi, and Susan Sandeman**

While intraocular lenses (IOL) are used to restore visual acuity in cataract patients, they are limited in their development as no clinically available lens can effectively mimic the accommodative function of the eye's natural lens. The optoelectronic properties of 2D transition metal carbides and/or nitrides (MXenes), including high electronic conductivity, optical transparency, flexibility, biocompatibility, and hydrophilicity, suggest potential use within an accommodating IOL. This study investigates the use of $Ti_3C_2T_x$ (MXene) as a transparent, conductive electrode to allow changes in optical power. $Ti_3C_2T_x$ is synthesized and spin-coated on hydrophobic acrylate IOLs, achieving a sheet resistance ranging from 0.2–1.0 kΩ sq^{-1} with 50–80% transmittance in the visible region. Human lens epithelial and monocytic cells show no cytotoxic nor inflammatory response to the coated lenses. An adjustable focus test cell is fabricated using a liquid crystal (LC) layer sandwiched between $Ti_3C_2T_x$ coatings on a solid support. Molecular reorientation of the LC layer, through an applied electric field, results in changes in optical power as objects viewed through the test cell appeared in and out of focus. This study is the first step toward the use of $Ti_3C_2T_x$ within an accommodative IOL design through demonstration of reversible, controlled, adjustable focus.

1. Introduction

Cataracts, formed by the aggregation of proteins on the crystalline lens of the eye, degrade visual acuity over time.[1] This age-related disorder accounts for the majority of the visually impaired population. The number of patients requiring cataract surgery will continue to rise with an increase in the average human life span. The eye's natural ability to vary optical power is known as accommodation or pseudophakia,[2,3] with optical power being the reciprocal of focal length measured in dioptres or m^{-1}. These changes in optical power are produced through ciliary muscle contraction and relaxation resulting in changes of lens curvature to provide continuous focus.[4] However, accommodation is lost as a result of cataract surgery when the eye's lens is removed and replaced with an intraocular lens (IOL). Even though the existing mechanisms of the eye, such as ciliary muscle contraction/relaxation and axial movement remain, the IOL of fixed optical power does not permit variable focus. IOL development is motivated to mimic more closely the eye's ability to retain focus at all lengths. Current accommodative intraocular lens (AIOL) approaches utilize the existing mechanisms of the eye. However, the main limitation associated with these methods is producing a reliable change in optical power. The ideal AIOL aims to have a controlled, reversible, and fast switching mechanism to seamlessly move from near to distant vision and vice versa. No clinically available AIOL reported to date truly restores accommodation.[5–7] In this article, a new transparent and conductive 2D material (MXene) was investigated for AIOL design.

A recent development in the field of optoelectronics is smart contact lenses.[8] They are wearable optoelectronic devices, proposed for the correction of presbyopia; an age-related disorder effecting the eye's accommodative function as the lens hardens and loses elasticity. These devices operate similarly to liquid crystal (LC) displays, where the optical anisotropy of a nematic LC is controlled by an electric field using transparent conductive electrodes (TCE).[9] LCs are mesogenic phases of matter, intermediate between solids and liquids and their average long-range orientational order is defined by their average direction, known as the director. Due to their orientational order, they have two refractive indices—parallel and perpendicular—that can be

E. J. Ward, Dr. M. K. Dymond, Dr. S. Sandeman
School of Pharmacy and Biomolecular Sciences
University of Brighton
Brighton, BN2 4GJ, UK
E-mail: S.Sandeman@brighton.ac.uk
Dr. J. Lacey
Rayner Intraocular Lenses Limited
The Ridley Innovation Centre
Worthing, BN14 8AQ, UK
Prof. C. Crua
Advanced Engineering Centre
University of Brighton
Brighton, BN2 4GJ, UK
Dr. K. Maleski, K. Hantanasirisakul, Prof. Y. Gogotsi
Department of Material Science and Engineering
A. J. Drexel Nanomaterials Institute
Drexel University
Philadelphia, PA 19104, USA
The ORCID identification number(s) for the author(s) of this article can be found under https://doi.org/10.1002/adfm.202000841.

DOI: 10.1002/adfm.202000841

manipulated through external stimuli such as, mechanical, electric, or magnetic fields, allowing molecular reorientation of the director. This allows switchable refractive indices making them useful for adjustable focus lens systems.[10] Many of the proposed smart contact lenses use indium tin oxide (ITO), a standard TCE, due to its characteristics of low sheet resistance and high optical transparency, coated on poly(methyl methacrylate) (PMMA).[11] However, the use of ITO comes with some limitations as it is brittle and therefore not suitable for wearable optoelectronic applications when flexibility is required.[12] 2D nanomaterials, with high flexibility and electronic conductivity, may be better suited Graphene variants, for example, have gained interest in wearable device applications owing to their optoelectronic properties and biocompatibility.[13–16] MXenes are a newer family of 2D transition metal carbides and nitrides, that have also shown potential for optoelectronic applications. These materials have a unique blend of mechanical, electrical, and physical properties including transparency in the visible spectrum, high electronic conductivity (up to 15000 S cm^{-1}), flexibility, hydroxide/oxide-like surface chemistry, and hydrophilicity.[17–20]

MXenes are synthesized from selective etching of layered precursors, such as ternary carbides and nitrides (MAX phases).[21] With the general formula $M_{n+1}AX_n$, M represents an early transition metal, A is an element from group 13 or 14 of the periodic table and X represents carbon and/or nitrogen.[17] MXenes can be produced through wet chemical approaches, selectively etching away the A-element, resulting in the formation of $M_{n+1}X_nT_x$ where T_x are terminating groups whose abundance and type are dependent on the etching process.[22] More than 30 MXenes have been synthesized, since their discovery in 2011, and many more variants are theorized to exist.[23–26] This family of materials has demonstrated outstanding potential in energy storage,[27,28] electromagnetic interference (EMI) shielding,[29,30] and water purification.[31,32] Even though MXene research for biomedical applications remains in its infancy, they have been used for a number of applications such as, diagnostic imaging,[33,34] biosensing,[35–37] as antibacterial materials,[38,39] and in theranostics.[40–42] The most investigated MXene, $Ti_3C_2T_x$, has shown low cytotoxicity to normal cells when compared to cancerous cells lines.[43]

Deposition techniques of MXenes, including spray-, spin-, and dip-coating, produce high-functioning transparent and flexible coatings.[24,44] For example, $Ti_3C_2T_x$ antennas that were bent through a series of different curvatures saw no change in performance or structure.[45] The study shows the flexibility and stability of the coatings, properties that are useful for electrode applications. $Ti_3C_2T_x$ electrodes for neural interfaces have been investigated for sensing applications demonstrating low impedance, high signal-to-noise ratio, and biocompatibility with regard to neuron cell viability.[46] However, MXenes have not yet been proposed for an AIOL design or any ophthalmic medical device application.

Herein, we describe the synthesis and characterization of $Ti_3C_2T_x$ colloidal solution. Once spin-coated onto a hydrophobic IOL (**Figure 1**a), its optoelectronic properties were investigated and biological interactions were assessed. As a proof of concept design, an adjustable focus lens was fabricated within a solid support. It was constructed with a LC layer sandwiched between $Ti_3C_2T_x$ spin-coated glass slides and, through electric field induced molecular reorientation, a change in refractive index and therefore optical power was observed (Figure 1b). The switchable focus demonstrates the incorporation of MXene for an adjustable focus lens. This is the first study investigating

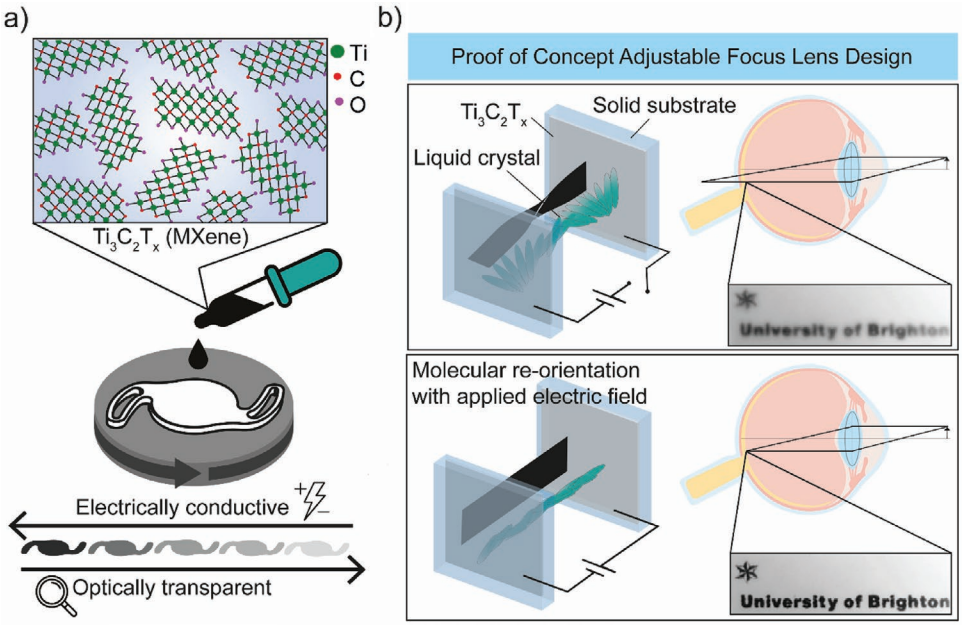

Figure 1. Accommodative intraocular lens (AIOL) design. a) A schematic of $Ti_3C_2T_x$ (MXene) spin coated onto an acrylate IOL (Rayner Intraocular Lenses Ltd, UK) showing fundamental properties of electrical conductivity and optical transparency. b) A schematic of a proof of concept design for an adjustable focus lens. The fabricated test cell was constructed with $Ti_3C_2T_x$ spin coated glass slides assembled to sandwich a liquid crystal (5CB) layer in twisted nematic orientation. With no electric field applied the image is out of focus. When the electric field is applied the image is in focus due to molecular reorientation of the liquid crystal layer.

the application of a 2D titanium carbide in optoelectronic AIOL design. Furthermore, the MXene fabricated IOL contributes to the field of ophthalmology and wearable electronics as currently no IOL designs involving MXenes have been explored.

2. Results and Discussion

2.1. Synthesis and Physical Characterization of $Ti_3C_2T_x$ (MXene)

$Ti_3C_2T_x$ was synthesized by chemical exfoliation of the MAX phase precursor, Ti_3AlC_2. Solvated lithium ions from the lithium fluoride (LiF) and hydrochloric acid (HCl) etchant facilitated the intercalation of multi-layered $Ti_3C_2T_x$ to delaminate into 2D $Ti_3C_2T_x$ flakes, resulting in stable colloidal solutions. A known volume of the solutions was vacuum-filtered to produce a free-standing film composed of $Ti_3C_2T_x$ flakes. The cross-section of the film was captured with scanning electron microscopy (SEM) (Figure S1, Supporting Information) showing the alignment of single flakes compacted as a result of the filtration. X-ray diffraction (XRD) patterns of the free-standing film along with the powdered precursor Ti_3AlC_2 (MAX) are shown in Figure S2, Supporting Information. The (002) peak of the Ti_3AlC_2 MAX powder and free-standing $Ti_3C_2T_x$ film are 9.5° and ≈7.1°. The interlayer spacing was calculated to be 18.6 and ≈25 Å, respectively. The increase observed in the *c* lattice parameter was a result of the removal of Al and the introduction of surface termination and intercalated water molecules. X-ray photoelectron spectroscopy (XPS) of the free-standing film was used to analyze the chemical composition of $Ti_3C_2T_x$ as shown in Figure S3, Supporting Information. Titanium and carbon were identified as core elements as well as oxygen and fluorine as terminating groups. Aluminum is absent in each analysis, consistent with the conversion of MAX to MXene. Dynamic light scattering (DLS) was used to provide flake size estimations. One peak was identified on the DLS distribution (Figure S4, Supporting Information) with an average size of 1250 nm and a polydispersity index (PDI) of 0.5. UV–vis spectroscopy was performed (Figure S5, Supporting Information), and a peak in the near infrared region was observed for $Ti_3C_2T_x$. Corresponding with the literature, the broad peak at 700–800 nm is characteristic of a transverse surface plasmon mode in $Ti_3C_2T_x$.[47] The extinction coefficient was calculated from a plot of absorbance versus concentration (inset of Figure S5, Supporting Information) as 31.34 L g^{-1} cm^{-1}.

2.2. Coating and Physical Characterization of $Ti_3C_2T_x$ Coated Lens

The key attributes of transparent electrodes are to be optically transparent and conductive, allowing the passage of light while permitting the flow of electrons. $Ti_3C_2T_x$ was deposited onto the lens and the coating's ability to perform as a TCE was evaluated. Commercially available, hydrophobic acrylate IOLs (Rayner IOL ltd) were used for this study. First, the lenses were treated with oxygen plasma to increase the hydrophilicity of the surface which improves the uniformity of the coatings. $Ti_3C_2T_x$ was deposited onto the treated lenses by spin-coating. The optical transmittance of the coated lenses showed a broad peak at 700–800 nm, consistent with the UV–vis peak observed for the colloidal solution as described in Section 2.1. By varying coating thickness, the optical transmittance can be optimized (**Figure 2**a). Nanoscale thickness of the coatings was optimized by a combination of varying the spin speed and concentration of the solution being coated and by layering the coatings. A numerical formula, $A = 0.005t$,[24] A being absorbance and t thickness in nm, was used to approximate the MXene coating thickness (Figure S6, Supporting Information).

$Ti_3C_2T_x$ coated lenses were evaluated as electrodes by measurement of sheet resistance. The bulk conductivity of the $Ti_3C_2T_x$ free-standing film (Figure S1, Supporting Information) was ≈6000 S cm^{-1}, indicating high quality of the 2D flakes produced. Sheet resistance of the coated lenses was measured using a four-point probe technique; the experimental setup, and calculations are shown in Figure S7, Supporting Information. Coatings with varied thicknesses were measured and their sheet resistance was found to range from 0.2–1.0 kΩ sq^{-1} with optical transmittance of 50–80% (Figure 2b). An effective means of evaluation for TCEs is through their electrical figure of merit (FoM) which is defined as the ratio between electrical conductivity (σ_{DC}) and optical conductivity (σ_{Op}).[48] The FoM for the MXene-coated lens was calculated as 1.8 (Figure S8, Supporting Information). The substrate surface could be a limiting factor with regards to increasing the FoM. When spin-coated, the centrifugal force orients the $Ti_3C_2T_x$ flakes in plane with the substrate that could increase resistance and affect electron flow. The $Ti_3C_2T_x$-coated IOLs were evaluated for optoelectronic performance as a TCE. Future efforts will be made to enhance performance for the desired high optical transparency and low sheet resistance.

The purpose of an IOL is to allow good visual acuity for the patient following the removal of a cataract. Visual acuity must not be diminished when a coating is introduced to the lens. Therefore, the $Ti_3C_2T_x$-coated lenses were assessed to determine the impact of the coating on lens' optical performance in terms of optical power and spatial resolution. Since IOLs are manufactured for the specific requirements of each individual patient, the axial length of the eye is measured to determine the optical power required. Standard characterization and quality tests that are used in the industrial manufacture of IOLs were performed. Here, no significant difference in optical power was observed on a series of lenses measured before and after coating (Figure 2c). Modulation transfer function (MTF) provides a universal metric based on a lens system's contrast and resolution abilities across the optic.[49] No significant difference was observed in MTF before and after coating (Figure 2d). The $Ti_3C_2T_x$ coatings did not significantly affect the optical performance or quality of the lens. This showcases the advantage of using $Ti_3C_2T_x$ as a conductive coating since it can provide sufficiently high electrical conductivity at low coating thicknesses and thus minimally affect the optical performance of the lens.

2.3. Biocompatibility of $Ti_3C_2T_x$ Coated Lens

To further assess the suitability of $Ti_3C_2T_x$ as a coating for AIOL design, the biocompatibility was evaluated through

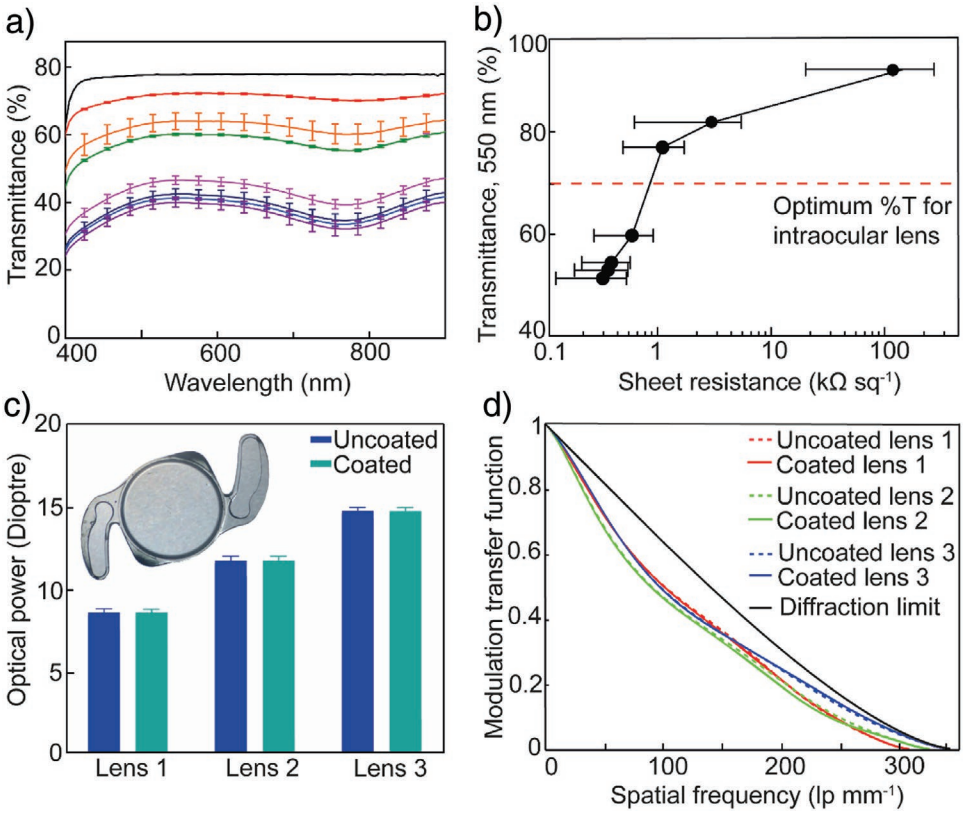

Figure 2. Optoelectronic characterization a) Transmittance spectra of $Ti_3C_2T_x$ coated lenses (black, no coating, colored etc. sequential coatings) mean ± SD, $n = 3$. b) Sheet resistance versus transmittance at 550 nm mean ± SEM, $n = 3$, error bars for transmittance are too small to be visible on the plot. c) Optical power measurement on 3 different lens powers before and after coating with $Ti_3C_2T_x$ for each type $n = 5$, mean ± SD, analyzed by one-way ANOVA, $p < 0.05$. Inset (c) Optical image of spin coated intraocular lens. d) Modulation transfer function (MTF) measurement on three different lens powers before and after coating with $Ti_3C_2T_x$ for each type $n = 5$. Both measurements made using a NIMO (NIMO TR0815, Lambda-X, Belgium).

cytotoxicity testing using (3-(4,5-dimethylthiazol-2-yl)-5-(3-carboxymethoxyphenyl)-2-(4-sulfophenyl)-2H-tetrazolium) MTS and lactate dehydrogenase (LDH) assays. The results of the MTS assay (**Figure 3**a) indicated no significant difference in percent cell viability for human lens epithelial cells (HLEs) incubated with $Ti_3C_2T_x$ coated IOLs when compared to the cell and lens only controls indicating no cytotoxic effects. Findings were supported by the data from the LDH assay (Figure 3b), showing no significant cytotoxic effects by $Ti_3C_2T_x$ coated IOLs compared to cell only controls. These findings demonstrate the cytocompatibility of $Ti_3C_2T_x$ coatings and their suitability for contact with ocular cell types. However, for IOL design, capsular and uveal biocompatibility is essential. Understanding the full biocompatibility profile for IOL applications requires assessment of potential interactions with inflammatory pathways which may be activated following exposure to a biomaterial. Since optoelectronic films such as $Ti_3C_2T_x$ have potential for electron transfer, it is thought that these materials may interact with biological systems with the ability to drive harmful processes such as oxidative stress through reactive oxygen species (ROS) production.[50] In order to explore this potential, both immunological activation studies and ROS production were investigated. Non-adherent THP-1 cells were used to investigate if $Ti_3C_2T_x$ coated IOLs induced oxidative stress by measuring the generation of ROS. No significant difference in ROS production throughout the study period was observed (Figure 3c). This demonstrates that under biological conditions, $Ti_3C_2T_x$ coatings do not provoke an increase in ROS production, supporting the MTS and LDH data indicating that the coatings were non-cytotoxic, and confirming the suitability of these nanomaterials for wider biological applications. The results of immunological cellular studies also supported this conclusion, with no increase in production of common ocular inflammatory cytokines IL-6, IL-8, and TNF-α by THP-1 monocytes in the presence of $Ti_3C_2T_x$ coated IOLs in contrast to LPS stimulated THP-1 controls (Figure 3d–f).

2.4. A Proof of Concept Accommodative Focus Lens Design

To assess the potential use of $Ti_3C_2T_x$ as a TCE in an adjustable focus lens system, a test cell was fabricated as a proof of concept design, (Figure S9, Supporting Information). The test cell, similar to a LC display, was constructed by a LC layer, of known thickness, sandwiched between $Ti_3C_2T_x$ spin-coated glass slides, with twisted nematic alignment (Figure 1b). By applying an electric field, a change in refractive index of the LC was observed due to the reorientation of molecules, producing a change in optical power of the lens. A typical thermotropic LC, 4'-Pentyl-4-cyanobiphenyl (5CB) was used. The

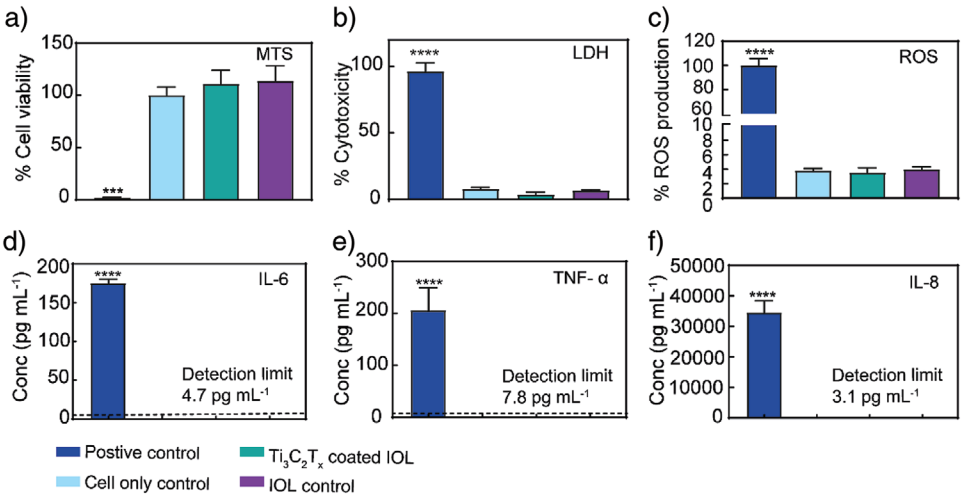

Figure 3. Biological evaluation for $Ti_3C_2T_x$ coated lenses a) % Cell viability via MTS assay for $Ti_3C_2T_x$ coated lens with HLE cell line, mean ± SEM, $n = 3$, $p < 0.05$. b) % Cytotoxicity by LDH assay for $Ti_3C_2T_x$ coated lens with HLE cell line, mean ± SEM, $n = 3$, $p < 0.05$. c) ROS activity of $Ti_3C_2T_x$ coated lens with THP-1 cell line, mean ± SEM, $n = 3$, $p < 0.05$. d–f) ELISA data of IL-6, TNF- α, and IL-8, respectively for $Ti_3C_2T_x$ coated lens with THP-1 cell line, mean ± SEM, $n = 3$, $p < 0.05$.

optical effects observed for 5CB are due to its nematic behavior at room temperature, positive dielectric anisotropy, and high birefringence. The alignment of the LCs director field defines the perpendicular (ordinary "n_o") or parallel (extraordinary "n_e") refractive index.[51] The refractive index of the test cell, with the electric field applied, was measured to be 1.7280 ± 0.0479 (mean ± SD, $n = 3$) at 24 °C, $\lambda = 405$ nm (Figure S10, Supporting Information). A study investigating the effects of temperature on the refractive indices of 5CB for a range of wavelengths of the EM spectrum found $n_e = 1.7232$ at 25.4 °C, $\lambda = 546$ nm,[52] confirming the test cell with the electric field applied experienced parallel orientation.

The optical effects of the test cell were observed showing focused and out of focus objects using the set up detailed in Section 4.6 and Figure S11, Supporting Information. As a means of quantifying the switchable focus of the test cell, data were captured and processed using a Laplacian operator for edge detection. Differential edge detection operators are used to provide edge information, for digital image analysis, through rapid changes in pixel greyscale intensity.[53] The operator compares the greyscale between neighboring pixels and reports the overall variance (σ^2); if the greyscale values are similar between pixels then it is assumed that at that point no edge is present.[54] For the purpose of this study, the variance of the image's pixel greyscale was used as a metric for focus, since an image that is in focus will have a higher degree of change in pixel greyscale than an out of focus image and therefore a higher computed variance value. The inset of **Figure 4**a shows two digital images taken with (top image) and without (bottom image) the 30 V electric field applied. It is clear from the image that it changed from out of focus to in focus state when the voltage was applied, as a result of the realignment of the LC. Figure 4a shows the histograms of each of the image's greyscale intensities. There are distinct differences between the plots for each image. The in focus state (electric field applied) shows a larger frequency distribution, spread over more dark pixels, whilst the out of focus state has less of a range. The corresponding variance values for the out of focus and in focus state are 3.7 and 24.3, respectively. For simplicity of image processing, the following investigations were performed on a series of small black lines (Figure S12, Supporting Information). Variance was plotted as a function of applied voltage as shown in Figure 4b. As voltage increased, a gradual increase in the variance value was observed, implying that the image became more in focus with the applied electric field. Fréedericksz transitions explain how the dielectric anisotropy of LCs allow molecular re-orientation when an electric field is applied.

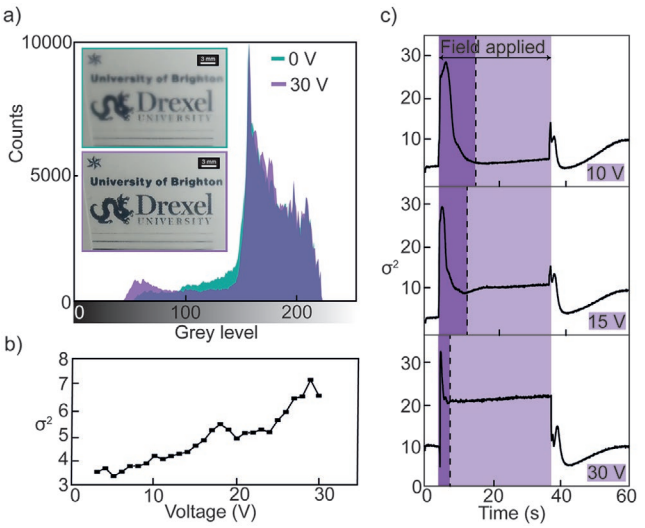

Figure 4. Digital image processing using the Laplacian operator for the proof of concept adjustable focus lens design a) Histograms of pixel greyscale for the inset (a) images of institute logos viewed through the fabricated test cell. b) Image processing to provide variance (σ^2) of image pixels greyscale intensity for a range of voltages. c) Image processing to provide variance (σ^2) of image pixels greyscale intensity for a range of voltages as a function of time, with the switching time (dark purple) and time the electric field was applied highlighted (light purple).

To investigate the dynamic of LC orientation, the variance value was plotted as a function of time at different applied voltages, as shown in Figure 4c. The time for LC reorientation was calculated by subtracting the time at which the minimum variance value was observed, from the time that the maximum variance value was observed. For 10, 15, and 30 V, the switching times were calculated as 2.30, 1.04, and 0.26 s, respectively, demonstrating a decrease in time taken for reorientation as the applied voltage was increased.

The purpose of the study was to achieve a change in optical power through a MXene/liquid crystal lens design. This is the framework for an AIOL design to allow optical changes as seamlessly as the natural lens. A number of factors could be investigated in further work to optimize the performance of the test cell. These include improvements in electrode efficiency through a reduction in the sheet resistance of the $Ti_3C_2T_x$ coating which can be achieved through an increase in the bulk conductivity of the initial $Ti_3C_2T_x$ solution. It has already been shown that $Ti_3C_2T_x$ free-standing films composed of larger flakes have greater conductivity than films produced with smaller flakes. These smaller flakes have lower sheet resistance, due to electron flow and less flake to flake electron hopping.[55] Larger $Ti_3C_2T_x$ flakes can be isolated after the delamination step described in Section 2.1.

Next, unwanted optical aberrations could be reduced by minimizing point defects at the substrate surface, ensuring uniformity of surface anchoring of the PVA alignment layer. The thickness of the LC layer determines the voltage required for reorientation, by decreasing the spacing between the electrodes and therefore the LC layer. This means less voltage is required. The threshold voltage required for reorientation of LC in test cell arrangements is a well-investigated topic and studies have shown that doping LC with nanoparticles, such as graphene oxide, decreases the voltage required to allow reorientation.[56] The data presented in this study shows the potential for the $Ti_3C_2T_x$ coating to act as a TCE for an adaptive focus lens application.

3. Conclusion

The first attempt to use a MXene thin film coating as an optically transparent electrode for an accommodative intraocular lens design was evaluated. The study demonstrates a synthesis and coating method by which a transparent, conductive $Ti_3C_2T_x$ thin film can be coated onto an acrylate polymer IOL surface using an approach which can be further optimized to increase electrical FoM. The study shows the first use of $Ti_3C_2T_x$ in an adjustable focus lens. Furthermore, $Ti_3C_2T_x$ coatings did not negatively affect human lens epithelial cell viability, stimulate upregulation of reactive oxygen species or inflammatory cytokine expression in THP-1 monocytes, demonstrating the biocompatibility of $Ti_3C_2T_x$ thin films coatings for this application. The $Ti_3C_2T_x$ coatings did not alter image quality of the lenses with respect to lens power or spatial resolution. The study demonstrates the use of $Ti_3C_2T_x$ as a TCE in the first step toward an accommodating lens design following further optimization of MXene properties for improved sensitivity.

4. Experimental Section

Reagents: MAX phase Ti_3AlC_2 (A.J. Drexel Nanomaterials Institute, Drexel University, USA), lithium fluoride (LiF) (powder 300 mesh) (Sigma-Aldrich, UK), hydrochloric acid (HCl) (Sigma-Aldrich, UK).

Synthesis of $Ti_3C_2T_x$ (MXene): Hydrofluoric acid (HF), formed in situ, when 0.8 g of LiF dissolved in 10 mL 9 M HCl. 0.5 g Ti_3AlC_2 was added gradually over 5 min, etched with continuous stirring for 24 h at 35 °C. Reaction byproducts were removed by washing with deionized (DI) water (200 mL) and repeatedly centrifuging (5 min, 3500 rpm) using an ALC PK 120R Centrifuge. Once a pH of 5–6 was achieved the sediment was redispersed and hand shaken for 15 min, then centrifuged for 1 h at 3500 rpm to delaminate. The delaminate product was decanted, and a known volume of the solution was vacuum-filtered and weighed to establish concentration (mg mL^{-1}). During storage the solution was frozen at −20 °C.

Physical Characterization of $Ti_3C_2T_x$ Solution: The $Ti_3C_2T_x$ solutions bulk composition was analyzed by XRD with a powder diffractometer (Rigaku SmartLab, USA) using CuKα radiation (λ = 1.54 Å) with θ–2θ continuous scan with 0.02° 2θ step size, 1 s step time, and 10×10 mm^2 window slit. Ultraviolet–visible (UV–vis) spectroscopy was carried out using an Evolution 201 UV–vis spectrophotometer (Thermo Scientific, USA) to characterize optical properties in the wavelength range of 200–1100 nm. Particle size analysis was carried out on MXene solutions using dynamic light scattering (DLS) (Zetasizer Nano ZS, Malvern Panalytical, UK). Scanning electron microscopy (SEM) (Zeiss Supra 50VP, Germany) was used to image MXene flakes using a MXene film as the sample produced by vacuum filtering at low concentration solution onto a porous membrane (Anodisk inorganic filter membrane, Whatman). No sputter coating was required for the samples. A four-point probe stand SR-4 (1 mm probe spacing) and Keithley SMU 2450 Source meter (Tektronix, USA) were used to measure the sheet resistance of the $Ti_3C_2T_x$ free-standing films produced. The bulk conductivity was calculated using the measured sheet resistance and the crossectional thickness measured with SEM.

$Ti_3C_2T_x$ Spin Coating onto an Intraocular Lens Material: In order to produce a uniform coating on a hydrophobic lens polymer substrate (Rayner Intraocular Lenses Ltd, UK), surface pre-treatment was required in the form of oxygen plasma using a Henniker plasma etcher (Henniker plasma, UK). The substrate was subject to a 3-min treatment of pure oxygen plasma at 100 W and 10 cm^3 min^{-1}. The treatment cleaned the surface and increased the hydrophilicity to allow the $Ti_3C_2T_x$ an adequate coating. 20 µL of a 5 mg mL^{-1} MXene solution was deposited on to the substrate. A two-step spin coating method was used with an Ossila spin coater (Ossila, UK), 5000 rpm for 2 min to evenly deposit the coating followed by 6000 rpm for 1 min to ensure drying of the coating.

Physical Characterization of $Ti_3C_2T_x$ Coated Lens: The properties of the coated lens surface were characterized by XPS (Physical Electronics VersaProbe 5000, USA) and SEM. XPS spectra were collected using an Al Kα X-ray beam. Dual beam stabilizer was used for charge neutralization. High-resolution scans were obtained with a pass energy of 23.5 eV. Spectral transmission of the coated lens was measured using a UV–vis spectrometer in the wavelength range of 300–1100 nm (Shimadzu, UV–vis Spectrophotometer, UV-2600, Japan) with an integrating sphere to collect any light scattered by the lens optic. The $Ti_3C_2T_x$ coatings were applied incrementally to the polymer lens (n = 3). Sheet resistance was measured using an electrical transport option (ETO) puck. A four-point probe orientation was made on the $Ti_3C_2T_x$ coating on the lens using silver wire and silver conductive paint. The puck was fitted to a circuit that was connected to the source meter described above. Three measurements were made per lens and the average values (n = 3) were reported. Lens quality was assessed through optical measurements of lens power and MTF using a NIMO measurement system (NIMO TR0815, Lambda-X, Belgium). These measurements were performed before and after deposition to ensure that the $Ti_3C_2T_x$ coating did not affect the lens optically or interfere with resolution or contrast.

Biocompatibility of the $Ti_3C_2T_x$ Coated Lens–Cell Viability: Cell viability following exposure to material leachate was assessed using the

CellTiter 96 AQueous One Solution Assay (MTS reagent) (Promega, USA). A human lens epithelial (HLE) cell line (B-3, ATCC CRL-11421) was purchased from the American Type Culture Collection (ATCC) and cultured in growth medium Minimum Essential Medium (MEM) supplemented with 20% FBS and 1% non-essential amino acids (NEAA) at 37 °C, 5% CO_2. Cells were passaged by standard trypsinization, plated at a seed density of 5 x 10^4 cells per well in a 96 well plate and were incubated at 37 °C, 5% CO_2 for 24 h. Material leachate was prepared using lenses coated with $Ti_3C_2T_x$, (detailed in Section 4.4). Coated lenses and controls were sterilized with ultraviolet (UV) light, allowing 60 min per side. Uncoated lenses were used as a negative control. Tin maleate coated polymer discs were cut to a surface area comparable to that of the lenses and were used as a positive control. Each material type was placed into the wells of a 48 well plate, 250 µL of medium was added, and plates were incubated at 37 °C, 5% CO_2 for 24 h. Following incubation, the material leachate was removed from the wells, 100 µL of it was then added to the plated cells. Plates were incubated at 37 °C, 5% CO_2 for a further 24 h. The MTS reagent was prepared according to manufacturer's instructions and 100 µL was used to replace the spent leachate media. After an incubation of 2 h at 37 °C, 5% CO_2, the absorbance at 490 nm was recorded using an ELx800 Universal Microplate reader (Biotek, USA). The experiment was repeated in triplicate. Cell number was calculated from a standard curve of cell density against absorbance at a wavelength of 490 nm. Percentage cell viability was calculated relative to the cell only control.

Biocompatibility of the $Ti_3C_2T_x$ Coated Lens–Cytotoxicity: Cytotoxicity was assessed using the CytoTox96 non-radioactive cytotoxicity assay measuring LDH release by lysed cells (Promega, USA). HLE cells were passaged by standard trypsinization, plated at a seed density of 5×10^4 cells per well in a 96 well plate and were incubated at 37 °C, 5% CO_2 for 24 h. Leachate media was prepared and introduced to the seeded cells as described in Section 2.6.1 and plates were incubated at 37 °C, 5% CO_2 for 24 h. 10 µL Lysis solution was added to half of the plate to establish maximum LDH release and plates were then incubated for 45 min, 50 µL of media from each well were transferred to a new plate and 50 µL of the substrate mix, prepared according to manufacturer's instructions, were then added to each well. The plate was incubated at room temperature in the dark for 30 min prior to addition of 50 µL of the stop solution to each well. The absorbance at a wavelength of 490 nm was recorded using an ELx800 Universal Microplate reader (Biotek, UK). The experiment was repeated in triplicate.

Biocompatibility of the $Ti_3C_2T_x$ Coated Lens–Immune Response: Cytokine production was quantified following incubation of coated lenses with monocyte THP-1 cells (ATCC TIB-202) using an enzyme-linked immunosorbent (ELISA) assay for interleukin 6 (IL-6), interleukin 8 (IL-8), and Tumor necrosis factor (TNF-α). The following ELISA assay kits were used: BD OptEIA Human IL-6 ELISA Kit II, BD OptEIA Human IL-8 ELISA Kit II and BD OptEIA Human TNF ELISA Kit II (BD Biosciences, USA). THP-1 cells were purchased from the ECACC and cultured in growth medium Roswell Park Memorial Institute (RPMI) with 10% FBS at 37 °C, 5% CO_2. The sterile, coated and uncoated lens samples were transferred into the wells of a 48 well plate. THP-1 cells were centrifuged and 300 µL of a 1×10^6 cells mL^{-1} cell suspension was added to each of the lens and control wells. 30 µL of lipopolysaccharide (LPS) (Sigma, UK) at a concentration 20 µg mL^{-1} was added to half of the plate at time zero as a positive control. The plate was incubated at 37 °C, 5% CO_2 for 24 h. Media from each well was removed and centrifuged with a Heraeus Pico 17 Microcentrifuge (Thermo Fisher Scientific, UK) at 800 g. The supernatant was analyzed by ELISA (BD Biosciences, UK) according to manufacturer's instructions using sample dilutions of 1 in 5, 1 in 5, and 1 in 600 for IL6, TNF-α, and IL8, respectively. Each experiment was repeated in triplicate.

Biocompatibility of the $Ti_3C_2T_x$ Coated Lens–Oxidative Stress: Sterilized, coated, and uncoated lenses in a 48 well plate were incubated with THP-1 cells to evaluate ROS production on exposure to $Ti_3C_2T_x$ coated lenses. Cells were stained with dichloro-dihydro-fluorescein diacetate (DCFH-DA) at a working concentration of 50 mM for 40 min followed by washing cycles with PBS until the cells were redispersed in FBS free RPMI. 300 µL of the cell suspension prepared at a seeding density of 3×10^5 cells mL^{-1} was added to each well. Hydrogen peroxide (H_2O_2) was added to half of the plate at a concentration of 0.8 mM at time zero as a positive control for induction of ROS. The plates were incubated at 37 °C, 5% CO_2 for 1 h. After incubation, 100 µL of the media was transferred into an opaque walled 96 well plate and fluorescence was measured at an excitation/emission wavelength of 485 nm/520 nm. Each experiment was repeated in triplicate.

A proof of Concept Accommodative Focus Lens Design: A test cell was fabricated when a LC layer was sandwiched between two $Ti_3C_2T_x$ spin-coated microscope slides. Before spin-coating the microscope slides (Superfrost plus microscope slides, VWR international, UK) were subject to oxygen plasma using a Henniker plasma etcher (Henniker plasma, UK) for 10 min at 100 W and 10 cm^3 min^{-1}. Next, 500 µL of a 5 mg mL^{-1} MXene solution was deposited on to the glass and a two-step spin coating method was used with an Ossila spin coater (Ossila, UK), 5000 rpm for 2 min followed by 6000 rpm for 1 min to ensure drying of the coating. MXene coated slides were placed in the oven at 80 °C for 24 h, to dry. A solution of 3% PVA (in water) was spin-coated onto the $Ti_3C_2T_x$ coated slide (1500 rpm for 1 min) and placed in the oven (80 °C) for 1 h. PVA coated $Ti_3C_2T_x$ slides were wiped with a microfiber cloth parallel to the long edge of the slides for alignment of the LC. A 50 µm film was used as a spacer and the glass slides were assembled (Figure S9, Supporting Information). Once constructed, the test cell was filled with LC (5CB (Sigma-Aldrich, UK)), by allowing capillary action to draw the 5CB into the void between the layers. Copper tape was placed on the $Ti_3C_2T_x$ coating and wires connected to a Keithley SMU 2450 Source meter (Tektronix, USA).

The refractive index of the test cell was measured both with and without applying an electric field, using a purpose-built in-line laser refractometer. The experimental setup (Figure S10, Supporting Information) was composed of a diode laser (Thorlabs CPS405, USA) emitting a beam at 405 nm, a 100 µm precision pinhole to clip the laser beam, translation and rotation stages to position the microscope slide assembly, and a CMOS camera (Basler ace acA1920-40gm, Germany) to record the beam's position shift. The position of the laser beam was recorded both with and without applying a 20 V electric field, allowing the beam shift (measured by sub-pixel affine image registration) to yield the change in refractive index using Snell's law.

The angle of the test cell holder relative to the laser beam was precisely measured by replacing the test cell with a sapphire optical flat and computing its angle from the induced laser beam shift. Once the angle of the test cell is known the only remaining unknown in the beam shift calculation is the refractive index of the LC layer in the test cell. Although the laser beam had a Gaussian profile, microscopic-scale refractive index gradients within the LC disrupted the radial energy distribution of the beam. The aberration was corrected by applying a frequency filter to the distorted beam profile images, so that the beam shift could be accurately measured.

Optical focus of the test cell was investigated when an electric field was applied, and the changes observed. An Olympus em10ii camera connected to a M.Zuiko 12-40 f2.8 pro lens was used to capture the data. Figure S11, Supporting Information, shows a schematic of the experimental setup, with the text being viewed through a lens, then through the test cell, by the camera. The object, lens, and test cell were all set at fixed distances in order to observe the expected change in optical power and therefore focal length. The electric field was applied to the test cell using a Keithley SMU 2450 Source meter (Tektronix, USA). A range of voltages were applied incrementally and held for 15 s before each image captured (Figure 4b). The investigation of the optical effects over time was performed on 10, 15, and 30 V, the voltage was applied for 30 s. The camera was set to record for 1 min to allow the initial switching time to be observed as well as the molecular relaxation time (Figure 4c).

The data were processed using a Laplacian differential function of the OpenCV 4.2.0 library written in Python (Figure S13, Supporting Information). All image frames were aligned prior to the processing. Examples are shown in Figure S14, Supporting Information, as controls to demonstrate the function of the operator with examples of high and

low variance where the images are in and out of focus respectively. An example of the image processing from the operator can be seen in Figure S12, Supporting Information.

Statistical Analysis: The statistical software package GraphPad Prism 7 was used for all statistical analyses. All biological data were analyzed using a Shapiro–Wilk normality test followed by a one-way ANOVA and a Tukey's multiple comparison test, $p < 0.05$. Optical power measurements were analyzed with the Shapiro–Wilk normality test followed by a paired *t*-test, $p < 0.05$. Errors are shown as standard deviation (SD) and standard error of the mean (SEM) where stated.

Supporting Information

Supporting Information is available from the Wiley Online Library or from the author.

Acknowledgements

This work was supported by a Medical Research Council Training Grant [MR/P015891/1]. The authors thank Mohamed Alhabeb and Tyler Mathis (Drexel) for providing MAX phase, XRD, and SEM characterization. XRD, XPS, and SEM were performed at Core Research Facilities (CRF) at Drexel University. The authors thank Nic Fusciardi for assistance with digital image processing.

Conflict of Interest

The authors declare no conflict of interest.

Keywords

accommodating intraocular lens, liquid crystals, MXene, nanomaterials, ophthalmic medical device, optoelectronic materials

Received: January 29, 2020
Revised: March 19, 2020
Published online:

[1] V. Gupta, M. Rajagopala, B. Ravishankar, *Indian J. Ophthalmol.* **2014**, *62*, 103.
[2] J. L. Alió, J. L. Alió del Barrio, A. Vega-Estrada, *Eye and Vision.* **2017**, *4*, 16.
[3] J. A. Venter, M. Pelouskova, B. M. Collins, S. C. Schallhorn, S. J. Hannan, *J. Cataract Refractive Surg.* **2013**, *39*, 1477.
[4] T. E. Lockhart, W. Shi, *Ergonomics* **2010**, *53*, 892.
[5] M. Walckling, R. Beck, O. Stachs, R. F. Guthoff, *Ophthalmology J.* **2018**, *3*, 29.
[6] J. L. Alio, A. Simonov, A. B. Plaza-Puche, A. Angelov, Y. Angelov, W. van Lawick, M. Rombach, *Am. J. Ophthalmol.* **2016**, *164*, 37.
[7] H. Siatiri, M. Mohammadpour, A. Gholami, E. Ashrafi, N. Siatiri, R. Mirshahi, *J. Current Ophthalmol.* **2017**, *29*, 274.
[8] H. E. Milton, P. B. Morgan, J. H. Clamp, H. F. Gleeson, *Opt. Express* **2014**, *22*, 8035.
[9] E. Lueder, in *Liquid Crystal Displays*, John Wiley & Sons, New York **2010**, pp. 57–82.
[10] J. Bailey, S. Kaur, P. B. Morgan, H. F. Gleeson, J. H. Clamp, J. C. Jones, *J. Phys. D: Appl. Phys.* **2017**, *50*, 485401.
[11] J. Bailey, P. B. Morgan, H. F. Gleeson, J. C. Jones, *Crystals* **2018**, *8*, 29.
[12] J. N. Coleman, P. J. King, U. Khan, M. Lotya, S. De, *ACS Nano* **2010**, *4*, 4238.
[13] X. Chen, F. Luo, M. Yuan, D. Xie, L. Shen, K. Zheng, Z. Wang, X. Li, L. Tao, *Adv. Funct. Mater.* **2019**, *29*, 1904706.
[14] K. Choi, H. G. Park, *ACS Nano* **2017**, *11*, 5223.
[15] C. Choi, M. K. Choi, S. Liu, M. S. Kim, O. K. Park, C. Im, J. Kim, X. Qin, G. J. Lee, K. W. Cho, M. Kim, E. Joh, J. Lee, D. Son, S.-H. Kwon, N. L. Jeon, Y. M. Song, N. Lu, D.-H. Kim, *Nat. Commun.* **2017**, *8*, 1664.
[16] T. Hwang, H.-Y. Kwon, J.-S. Oh, J.-P. Hong, S.-C. Hong, Y. Lee, H. Ryeol Choi, K. Jin Kim, M. Hossain Bhuiya, J.-D. Nam, *Appl. Phys. Lett.* **2013**, *103*, 023106.
[17] B. Anasori, M. R. Lukatskaya, Y. Gogotsi, *Nat. Rev. Mater.* **2017**, *2*, 16098.
[18] Z. Fu, N. Wang, D. Legut, C. Si, Q. Zhang, S. Du, T. C. Germann, J. S. Francisco, R. Zhang, *Chem. Rev.* **2019**, *119*, 11980.
[19] A. Lipatov, H. Lu, M. Alhabeb, B. Anasori, A. Gruverman, Y. Gogotsi, A. Sinitskii, *Sci. Adv.* **2018**, *4*, eaat0491.
[20] H. Kim, H. N. Alshareef, *ACS Mater. Lett.* **2020**, *2*, 55.
[21] B. Anasori, Y. Gogotsi, *2D Metal Carbides and Nitrides (MXenes)* (Eds: B. Anasori, Y. Gogotsi), Springer, Berlin **2019**.
[22] M. Alhabeb, K. Maleski, B. Anasori, P. Lelyukh, L. Clark, S. Sin, Y. Gogotsi, *Chem. Mater.* **2017**, *29*, 7633.
[23] M. Naguib, M. Kurtoglu, V. Presser, J. Lu, J.-J. Niu, M. Heon, L. Hultman, Y. Gogotsi, M. W. Barsoum, *Adv. Mater.* **2011**, *23*, 4248.
[24] K. Hantanasirisakul, M.-Q. Zhao, P. Urbankowski, J. Halim, B. Anasori, S. Kota, C. E. Ren, M. W. Barsoum, Y. Gogotsi, *Adv. Electron. Mater.* **2016**, *2*, 1600050.
[25] B. Anasori, Y. Xie, M. Beidaghi, J. Lu, B. C. Hosler, L. Hultman, P. R. C. Kent, Y. Gogotsi, M. W. Barsoum, *ACS Nano* **2015**, *9*, 9507.
[26] K. Hantanasirisakul, Y. Gogotsi, *Adv. Mater.* **2018**, *30*, 1804779.
[27] Y.-Y. Peng, B. Akuzum, N. Kurra, M.-Q. Zhao, M. Alhabeb, B. Anasori, E. C. Kumbur, H. N. Alshareef, M.-D. Ger, Y. Gogotsi, *Energy Environ. Sci.* **2016**, *9*, 2847.
[28] M. R. Lukatskaya, S. Kota, Z. Lin, M.-Q. Zhao, N. Shpigel, M. D. Levi, J. Halim, P.-L. Taberna, M. W. Barsoum, P. Simon, Y. Gogotsi, *Nat. Energy* **2017**, *2*, 17105.
[29] F. Shahzad, M. Alhabeb, C. B. Hatter, B. Anasori, S. Man Hong, C. M. Koo, Y. Gogotsi, *Science* **2016**, *353*, 1137.
[30] R. Bian, G. He, W. Zhi, S. Xiang, T. Wang, D. Cai, *J. Mater. Chem. C* **2019**, *7*, 474.
[31] K. Rasool, R. P. Pandey, P. A. Rasheed, S. Buczek, Y. Gogotsi, K. A. Mahmoud, *Mater. Today* **2019**, *30*, 80.
[32] J. Saththasivam, K. Wang, W. Yiming, Z. Liu, K. A. Mahmoud, *RSC Adv.* **2019**, *9*, 16296.
[33] X. Yu, X. Cai, H. Cui, S. W. Lee, X. F. Yu, B. Liu, *Nanoscale* **2017**, *9*, 17859.
[34] Q. Xue, H. Zhang, M. Zhu, Z. Pei, H. Li, Z. Wang, Y. Huang, Y. Huang, Q. Deng, J. Zhou, S. Du, Q. Huang, C. Zhi, *Adv. Mater.* **2017**, *29*, 1604847.
[35] L. Wu, X. Lu, Z. Wu, Y. Dong, X. Wang, S. Zheng, J. Chen, *Biosens. Bioelectron.* **2018**, *107*, 69.
[36] S. Kumar, Y. Lei, N. H. Alshareef, K. N. Salama, *Biosens. Bioelectron.* **2018**, *121*, 243.
[37] S. J. Kim, H.-J. Koh, C. E. Ren, O. Kwon, K. Maleski, S.-Y. Cho, B. Anasori, C.-K. Kim, Y.-K. Choi, J. Kim, Y. Gogotsi, H.-T. Jung, *ACS Nano* **2018**, *12*, 986.
[38] K. Rasool, K. A. Mahmoud, D. J. Johnson, M. Helal, G. R. Berdiyorov, Y. Gogotsi, *Sci. Rep.* **2017**, *7*, 1598.
[39] K. Rasool, M. Helal, A. Ali, C. E. Ren, Y. Gogotsi, K. A. Mahmoud, *ACS Nano* **2016**, *10*, 3674.
[40] Z. Liu, M. Zhao, H. Lin, C. Dai, C. Ren, S. Zhang, W. Peng, Y. Chen, *J. Mater. Chem. B* **2018**, *6*, 3541.

[41] X. Han, X. Jing, D. Yang, H. Lin, Z. Wang, H. Ran, P. Li, Y. Chen, *Theranostics* **2018**, *8*, 4491.
[42] G. Liu, J. Zou, Q. Tang, X. Yang, Y. Zhang, Q. Zhang, W. Huang, P. Chen, J. Shao, X. Dong, *ACS Appl. Mater. Interfaces* **2017**, *9*, 40077.
[43] A. M. Jastrzębska, A. Szuplewska, T. Wojciechowski, M. Chudy, W. Ziemkowska, L. Chlubny, A. Rozmysłowska, A. Olszyna, *J. Hazard. Mater.* **2017**, *339*, 1.
[44] P. Salles, D. Pinto, K. Hantanasirisakul, K. Maleski, C. E. Shuck, Y. Gogotsi, *Adv. Funct. Mater.* **2019**, *29*, 1809223.
[45] Y. Gogotsi, A. Sarycheva, A. Polemi, Y. Liu, B. Anasori, K. Dandekar, *Sci. Adv.* **2018**, *4*, eaau0920.
[46] N. Driscoll, A. G. Richardson, K. Maleski, B. Anasori, O. Adewole, P. Lelyukh, L. Escobedo, D. K. Cullen, T. H. Lucas, Y. Gogotsi, F. Vitale, *ACS Nano* **2018**, *12*, 10419.
[47] J. K. El-Demellawi, S. Lopatin, J. Yin, O. F. Mohammed, H. N. Alshareef, *ACS Nano* **2018**, *12*, 8485.
[48] S. De, J. N. Coleman, *ACS Nano* **2010**, *4*, 2713.
[49] G. D. Boreman, in *Modulation Transfer Function in Optical and Electro-optical Systems*, SPIE Press, Bellingham, WA **2001**, p. 120.
[50] T. Dutta, R. Sarkar, B. Pakhira, S. Ghosh, R. Sarkar, A. Barui, S. Sarkar, *RSC Adv.* **2015**, *5*, 80192.
[51] M. Schadt, *Annual Rev. Mater. Sci.* **1997**, *27*, 305.
[52] J. Li, *Refractive Indices Of Liquid Crystals And Their Applications In Display And Photonic Devices*, University of Central Florida, Florida **2005**.
[53] S. Y. Lee, Y. Kumar, J. M. Cho, S. W. Lee, S. W. Kim, *IEEE Transact. Circuits Systems Video Technol.* **2008**, *18*, 983.
[54] X. Wang, *IEEE Transactions on Pattern Analysis and Machine Intelligence* **2007**, *29*, 886.
[55] K. Maleski, C. E. Ren, M.-Q. Zhao, B. Anasori, Y. Gogotsi, *ACS Appl. Mater. Interfaces* **2018**, *10*, 24491.
[56] G. B. Hadjichristov, Y. G. Marinov, A. G. Petrov, L. Marino, N. Scaramuzza, *J. Phys.: Conf. Ser.* **2016**, *682*, 012015.